Controlling Wavebreaking in Dispersive Hydrodynamic Media

Dalton V. Anderson[12]†, Mark A. Hoefer [1] and Michelle D. Maiden[1]

[1]Department of Applied Mathematics, University of Colorado, Boulder, CO 80302, USA

[2]Department of Aerospace Engineering, University of Colorado, Boulder, CO 80302, USA

(Received xx; revised xx; accepted xx)

Dispersive hydrodynamic systems exhibit a rich variety of behavior, depending on the initial value problem considered. However, many such systems can only be experimentally controlled at one boundary. Here, a method is presented for generating an initial condition via a boundary value problem formulation for nonlinear dispersive partial differential equations, which model such systems. The conduit equation is chosen due to its high fidelity to physical experiments. The dispersionless limit of the conduit equation is taken and evolved backwards in time from the desired initial condition of a step increase of a constant background at a chosen point in space and time. This method is tested for various step sizes and positions of the step. Experiments on this method agree well with theory, having an upper bound of 10%, which is consisten with other conduit experiments.

1. Introduction

Dispersive shock waves (DSWs) are coherent structures that exhibit the interplay of nonlinearity and dispersion. A DSW is an expanding, oscillating train of amplitude-ordered nonlinear waves composed of a large amplitude solitary wave adjacent to a monotonically decreasing wave envelope that terminates with a packet of small amplitude dispersive waves. These structures are pervasive in dispersive hydrodynamic systems, having been observed in quantum systems (ultra-cold atoms Dutton *et al.* (2001-07); Hoefer *et al.* (2006-08), semiconductor cavities Amo *et al.* (2011), electron beams Mo *et al.* (2013)), nonlinear optics Rothenberg & Grischkowsky (1989), geophysical fluids Hammack & Segur (1978); Farmer & Armi (1999), and rarefied plasma Taylor *et al.* (1970). However, experimental generation and analysis of DSWs remains a difficult and expensive problem in many of these systems, constrained by expensive laboratory setups Dutton *et al.* (2001-07); Hoefer *et al.* (2006-08); Mo *et al.* (2013); Hammack & Segur (1978) challenging field studies Farmer & Armi (1999), difficulties in capturing dynamical information Rothenberg (1991); Dutton *et al.* (2001-07); Hoefer *et al.* (2006-08), complex physical modeling Farmer & Armi (1999), or a loss of coherence due to multi-dimensional instabilities Dutton *et al.* (2001-07); Amo *et al.* (2011) or dissipation Taylor *et al.* (1970); Mo *et al.* (2013).

Many of these difficulties have been overcome by utilizing a model dispersive hydrodynamics system: the conduit system. This system enables high fidelity studies of large amplitude DSWs, which are found to agree quantitatively with nonlinear wave averaging or Whitham theory Whitham (1974); Gurevich & Pitaevskii (1974); Lowman & Hoefer (2013-08); Maiden *et al.* (2016). However, the conduit system can only be controlled at one boundary, which makes the initial condition DSW problem difficult to study. Here, we report on a mathematical tool that is a feasible way to achieve wavebreaking away from

† Email address for correspondence: dalton.anderson@colorado.edu

boundary effects. We take the dispersionless limit of the conduit equation and evolve the step initial condition backwards in time. The resulting solution can be used as a boundary condition for the conduit equation and evolved forwards in time to yield the desired step in the full conduit system.

The following paper is organized as follows. Section 2 is the theoretical section and includes background information on the conduit equation and the mathematical procedure for converting the initial value problem to a boundary value problem. Section 3 is the experimental section and covers both numerical and experimental methods and analysis. Section 4 is a discussion of the major results of the previous two sections, and conclusions are in Section 5.

2. Theory

2.1. *Conduit Equation*

Conduits generated by the low Reynolds number, buoyant dynamics of two miscible fluids with differing densities and viscosities were first studied in the context of geological and geophysical processes Whitehead & Luther (1975). Here, we focus on viscous fluid conduits, which can be realized physically with glycerine for the exterior fluid, and glycerin diluted with water and dyed as the interior fluid [I am removing all mentions of corn syrup, as I believe all results presented are glycerine.] Olson & Christensen (1986); Scott *et al.* (1986-02); Whitehead & Helfrich (1988-11); Maiden *et al.* (2016). Perturbations around a constant background conduit with the assumptions of long-wavelength, slow-time, and slow-space result in the conduit equation, a (1+1)-D dispersive hydrodynamic equation with a nonlinear, nonlocal dispersive term Lowman & Hoefer (2013-08). This paper focuses on the realization of the Gurevich-Pitaevskii (GP) problem Gurevich & Pitaevskii (1974), a standard textbook problem for the study of DSWs El & Hoefer (2016), for the conduit equation

$$A_t + (A^2)_z - (A^2(A^{-1}A_t)_z)_z = 0. \tag{2.1}$$

This equation approximately governs the evolution of the circular interface with cross-sectional area A, in vertical space z and time t. This interface separates a light, viscous fluid rising buoyantly through a heavy, more viscous fluid at small Reynolds numbers in the long-wavelength, slow-time regime Scott *et al.* (1986-02); Lowman & Hoefer (2013-08). Here, the GP problem is the study of the dispersive hydrodynamics of an initial step increase in conduit area

$$A(z,t) = \begin{cases} A_1, & z \geqslant z_b \\ A_2, & z < z_b \end{cases}, \tag{2.2}$$

for some $A_2 > A_1$. Note that since the conduit equation obeys the scaling invariance

$$\tilde{A} = A/A_0, \quad \tilde{z} = A_0^{-1/2} z, \quad \tilde{t} = A_0^{1/2} t, \tag{2.3}$$

this is equivalent to studying

$$A(z,t) = \begin{cases} 1, & z \geqslant z_b \\ A_b, & z < z_b \end{cases}, \tag{2.4}$$

where $A_b = A_2/A_1 > 1$.

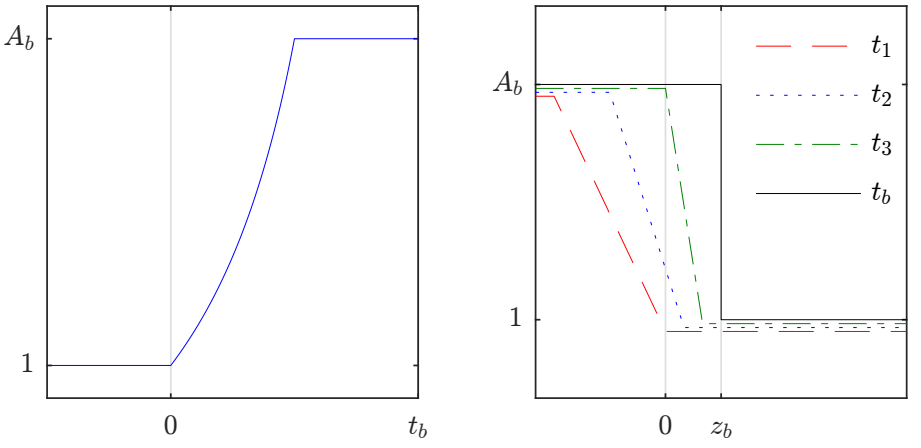

(a) Profile in t (b) Profile in z

FIGURE 1. (a) Dimensional version of the boundary condition Eq. 2.8. (b) Evolution of the rescaled piecewise rarefaction wave Eq. 2.8. Note as time moves forward, the wave approaches the desired step.

2.2. *Inviscid Burgers Equation*

To implement our method, we assume prior to DSW breaking, dispersive behavior is minimal. Intuitively, this assumption is valid because the GP problem connects two constant states, so no oscillitory behavior is observed. Therefore, we can safely neglect the dispersive term, $(A^2(A^{-1}A_t)_z)_z$, and focus on the inviscid Burgers Equation

$$u_\tau + \left(u^2\right)_\zeta = 0 \tag{2.5}$$

Here, we consider two main solution families of Eq. 2.5: constants and the self-similar solution $u(\zeta,\tau) = \frac{\zeta}{2\tau}$, called the rarefaction wave solution. This solution family is unbounded in u, thus in order to make the problem physical, we define a piecewise solution that connects two constant states $u_- < u_+$ with the rarefaction wave solution

$$u(\zeta,\tau) = \begin{cases} u_- & : \zeta \leqslant 2u_-\tau \\ \frac{\zeta}{2\tau} & : 2u_-\tau \leqslant \zeta \leqslant 2u_+\tau \\ u_+ & : \zeta \geqslant 2u_+\tau \end{cases}, \tag{2.6}$$

Although Eq. 2.6 is not differentiable everywhere, it is a weak solution of Eq. 2.5.

The substitution to convert this solution into the physical coordinate system is

$$\begin{gathered} \zeta = -(z - z_b), \quad \tau = -(t - t_b), \quad t_b = \tfrac{z_b}{2} \\ u_- = 1, \qquad\qquad\qquad u_+ = A_b \end{gathered} \tag{2.7}$$

Then the requisite boundary condition for Eq. 2.1 has the form

$$A(0,t) = \begin{cases} 1 & : t \leqslant 0 \\ (1 - 2t/z_b)^{-1} & : 0 < t/z_b < \frac{(A_b-1)}{2A_b} \\ A_b & : t/z_b \geqslant \frac{(A_b-1)}{2A_b} \end{cases}. \tag{2.8}$$

An example of this solution and its evolution is shown in Fig. 1.

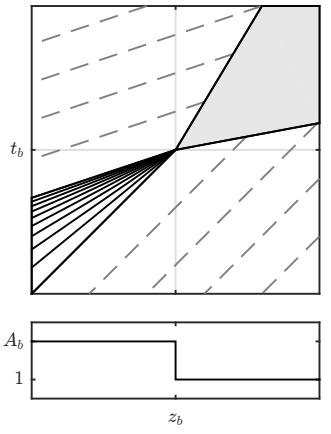

FIGURE 2.

2.2.1. *Dimensionalization*

[Is this section necessary? Could remove.] Next, we rescale Eq. 2.8 from the nondimensional conduit equation (tilded variables) to physical parameters (plain variables). Following the scaling given in Lowman & Hoefer (2013-08), denote by $f^{(i,e)}$ as the fluid property f for the interior or exterior fluid, μ as a fluid's dynamic viscosity, and ρ as its density. Then defining R_0 as the (dimensional) conduit radius, and Q_0 as the (dimensional) flow rate, we have

$$\begin{gathered}
\Delta = \rho^{(e)} - \rho^{(i)} \qquad \varepsilon = \frac{\mu^{(i)}}{\mu^{(e)}}, \qquad \alpha = \left(\frac{2^7 \mu^{(i)}}{\pi g \Delta}\right)^{1/4} \\
\tilde{R} = R/L, \qquad \tilde{z} = \varepsilon^{1/2} z/L, \qquad L = R_0/\sqrt{8} \\
\tilde{t} = \varepsilon^{1/2} t/T, \quad T = \frac{\sqrt{8}\mu^{(i)}}{g R_0 \Delta} \\
\tilde{u} = u/U, \qquad U = \frac{g R_0^2 \Delta}{8\mu^{(i)}} \\
\tilde{A} = A/A_0, \quad A_0 = \frac{\alpha^2 Q_0^{1/2}}{32}
\end{gathered} \tag{2.9}$$

Then rescaling 2.8 results in a volumetric flow rate profile with an area ratio of A_b and a predicted break height of z_b

$$Q(t) = Q_0 \begin{cases} 1 & : t \leqslant 0 \\ (1 - 2\frac{U}{z_b} t)^{-2} & : 0 < \frac{U}{z_b} t < \frac{(A_b - 1)}{2A_b} \\ A_b^2 & : \frac{U}{z_b} t \geqslant \frac{(A_b - 1)}{2A_b} \end{cases}. \tag{2.10}$$

2.3. *Generalization of Technique*

This method of neglecting the dispersive term can be used to generate a variety of initial conditions. In Figs. 2 & 3, we show characteristic plots based on the dispersionless approach to generate a DSW in Fig. 2, a box in Fig. 3(a), a triangle in Fig. 3(b), and an N-wave in Fig. 3(c). [Dalton, please add equations for these ICs and captions to the figures. Potentially combine Figs. 2 and 3 to save space. Are we adding the experimental versions here or in Results?]

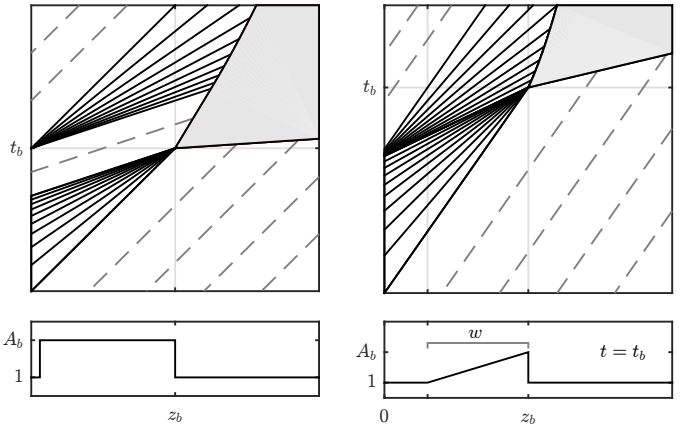

(a) box (b) triangle

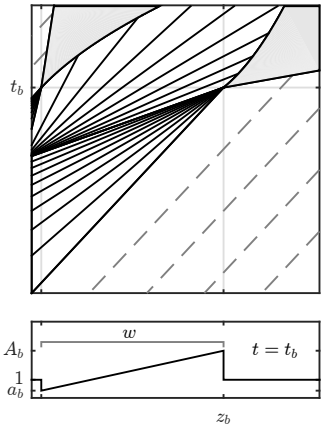

(c) N

FIGURE 3.

3. Experiment

3.1. *Setup*

The experimental apparatus shown in Fig. 4(a) consists of a square acrylic column with dimensions 4 cm × 4 cm × 92 cm; the column is filled with a highly viscous, transparent, exterior fluid - either corn syrup or glycerine. A nozzle is installed at the base of the column to allow for the injection of the interior fluid. To eliminate surface tension effects, the interior fluid is a solution of the exterior fluid (glycerine or corn syrup), deionized water, and black food coloring. Resultantly, the interior fluid has both lower density and viscosity than the exterior fluid ($\mu^{(i)} \ll \mu^{(e)}$, $\rho^{(i)} < \rho^{(e)}$).

Interior fluid is drawn from a separate reservoir and injected through the nozzle via a high precision piston pump controlled by a computer. The interior fluid rises buoyantly due to the density difference between interior and exterior fluids. By injecting at a constant rate, a vertically uniform fluid conduit is established. This "fluid conduit" is

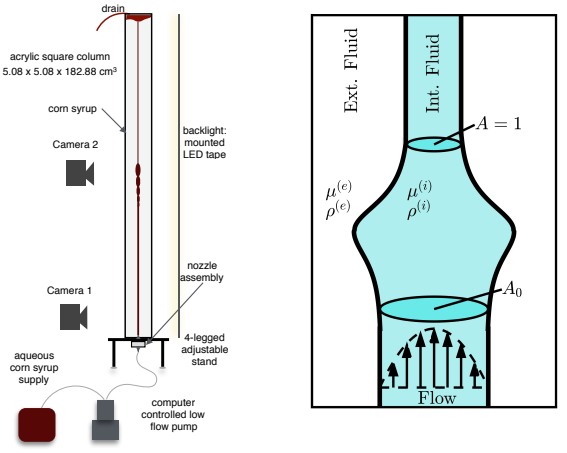

(a) (b)

FIGURE 4. (a) Schematic of the experimental setup. [Add ruler? Add computer connected to pump?] (b) Schematic of the conduit near $t = t_b$. Note that dispersion causes the step to "smooth out".

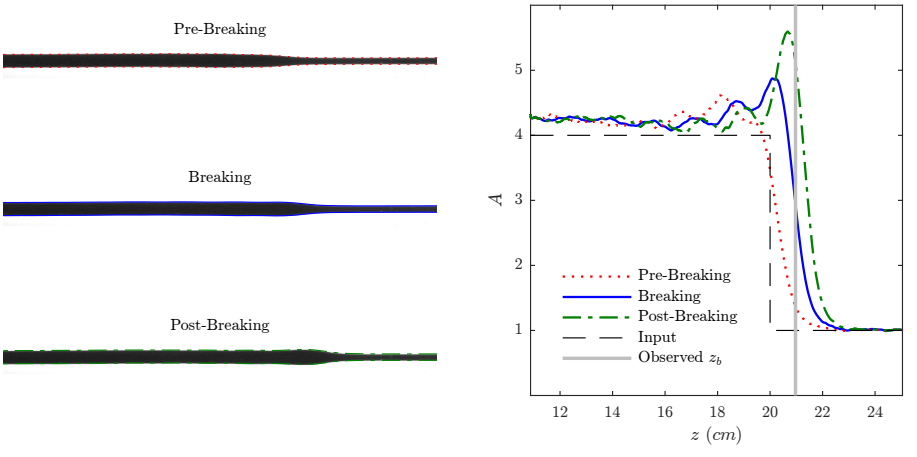

(a) (b)

FIGURE 5. (a) Processed images from a glycerine trial with $\mu^{(i)} = 72 \pm 1$cP, $\rho^{(i)} = 1.222 \pm 0.001$g/cm^3, $\mu^{(e)} = 1190 \pm 20$cP, $\rho^{(e)} = 1.262 \pm 0.001$g/cm^3, and $Q_0 = 0.25 \pm 0.01$ml/min. The grayscale images are overlayed with the extracted conduit edges and the conduit centerline. (b) Area plot corresponding to the images in (a). The vertical line indicates the step front, as found by the algorithm in 3.2.

referred to as the background conduit. Data acquisition is done using a high resolution camera equipped with a macro lens at the predicted break height. A ruler is positioned beside the column to determine the observed break height.

3.2. *Methods*

For each trial, a volumetric flow rate profile $Q(t)$ is generated using Eq. 2.10 for the chosen z_b and A_b. The predicted time of breaking, t_b, is $t_b = z_b/2U$. The camera takes several high-resolution images before, during, and after the time of breaking. A schematic of the conduit near the height and time of breaking is shown in Fig. 4(b). After breaking occurs, the pump is reduced to the background rate Q_0, and the conduit is left to equilibrate before the next trial.

The images from the camera are processed in MATLAB to extract the conduit edges (Fig. 5(a)) by taking a horizontal row of pixels and calculating the maximum and minimum derivatives for each row. As the background is white and the conduit is black, this finds the approximate boundary. The data is then sent through a low-pass filter to reduce noise from the pixelation of the photograph and any impurities (such as bubbles) in the exterior fluid.

After converting to area and rescaling the initial background area to unity, we then determine the experimental breaking height z_b and time t_b. Note that near the point of breaking, dispersion is no longer negligible; as a result, a Riemann step is never reailzed in the conduit system. Instead, we observe the initialization of a DSW as seen in Fig. 5(b). Therefore, an alternative definition of breaking must be implemented.

Turning to numerical simulations, we developed a robust method using the slope of the wave front. We observe an inflection point in the slope over time that roughly corresponds to the expected breaking time, t_b. Then, we interpolate the conduit area to $t = t_b$ and define breaking as halfway between the maximum (leading wave height) and minimum (leading constant conduit) of the conduit.

[Is it necessary to explain Uncertainty Quantification? Used textbook method.] [Note: We did NOT rescale z_b to counteract for viscosity error.]

3.3. *Wavebreaking Control*

- z_b vs A_b,Q_+
- [t_b vs the same]
- Corn Syrup vs glycerine
- Interpretation of Deviation
- Numerics

For glycerine, 15 trials were taken over the course of four hours. The main results of this experiment are how close the predicted breaking heights and times ($z_{b,in}$ and $t_{b,in}$) are to those experimentally observed ($z_{b,out}$ and $t_{b,out}$) [Should we also compare expected/observed A_b?]. These results are shown for glycerine in Fig. 6, comparing theory, numerics, and experiment for the breaking height (a) and the breaking time (b). In general, small A_b and large z_b had the worst error, but almost all experiments were under 10%.

3.4. *Characteristic control*

[DALTON: Before this can be written, we need: formulae for the boundary conditions, contour plots with experimental data added.]

4. Discussion

Overall, we see high fidelity between the expected and observed breaking heights and times. The regions of large error in parameter space are likely due to a breakdown in our initial assumption that nonlinearity dominates over dispersion. For small A_b, nonlinearity

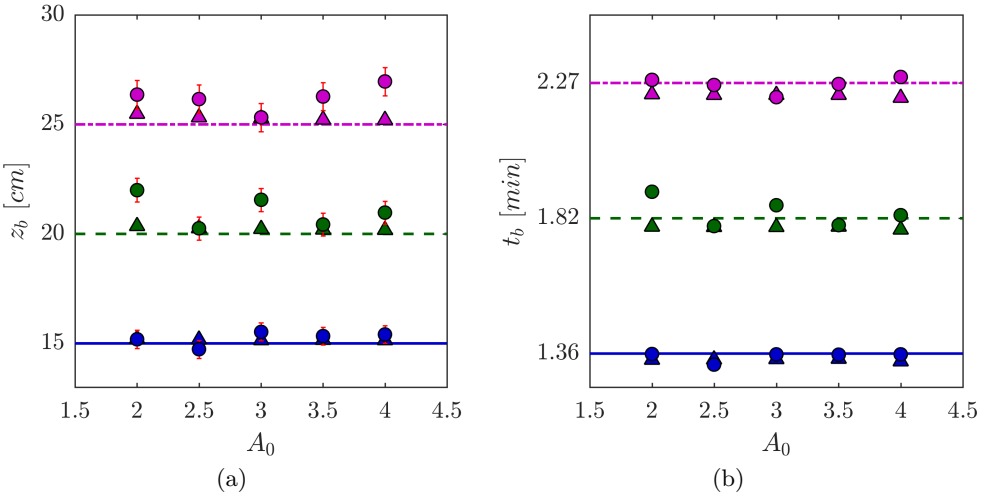

FIGURE 6. Comparison of dispersionless theory (lines), full conduit equation numerics (triangles) and glycerine experiments (circles) for the step initial condition. (a) Break height results for glycerine experiments as a function of expected break height and A_b, with the same fluid parameters as those in Fig. 5. (b) Break time results for those same experiments. Note the breaking time error is smaller than the symbols used. [Should we report these in seconds instead?]

does not have as large an effect as for other area ratios, and for large z_b, dispersion has more time to have a significant effect on the evolution of the boundary condition. This argument is all the more compelling because we see similar trends in the numerical data.

5. Conclusion

Using the dispersionless limit of a dispersive hydrodynamic system is an excellent approximation for non-oscillatory regions. By generating boundary conditions using this assumption, we are able to approximate a desired initial condition to 10% accuracy. This method could be used for a variety of nonlinear dispersive systems for more accurate analysis of dispersive shock waves or other hydrodynamic structures that evolve from initial conditions.

REFERENCES

AMO, A., PIGEON, S., SANVITTO, D., SALA, V. G., HIVET, R., CARUSOTTO, I., PISANELLO, F., LEMNAGER, G., HOUDR, R., GIACOBINO, E, CIUTI, C. & BRAMATI, A. 2011 Polariton superfluids reveal quantum hydrodynamic solitons. *Science* **332** (6034), 1167 –1170.

DUTTON, Z., BUDDE, M., SLOWE, C. & HAU, L. 2001-07 Observation of quantum shock waves created with ultra- compressed slow light pulses in a bose-einstein condensate. *Science* **293** (5530), 663.

EL, G. A. & HOEFER, M. A. 2016 Dispersive shock waves and modulation theory. *Physica D: Nonlinear Phenomena* .

FARMER, DAVID & ARMI, LAURENCE 1999 The generation and trapping of solitary waves over topography. *Science* **283** (5399), 188–190.

GUREVICH, A. V. & PITAEVSKII, L. P. 1974 Nonstationary structure of a collisionless shock wave. *JETP* **38** (2), 291–297, translation from Russian of A. V. Gurevich and L. P. Pitaevskii, Zh. Eksp. Teor. Fiz. 65, 590-604 (August 1973).

Hammack, Joseph L. & Segur, Harvey 1978 The korteweg-de vries equation and water waves. part 3. oscillatory waves. *J. Fluid Mech.* **84** (2), 337–358.

Hoefer, M., Ablowitz, M., Coddington, I., Cornell, E., Engels, P. & Schweikhard, V. 2006-08 Dispersive and classical shock waves in bose-einstein condensates and gas dynamics. *Phys. Rev. A* **74** (2), 023623.

Lowman, N. K. & Hoefer, M. A. 2013-08 Dispersive hydrodynamics in viscous fluid conduits. *Phys. Rev. E* **88** (2), 023016.

Maiden, Michelle D., Lowman, Nicholas K., Anderson, Dalton V., Schubert, Marika E. & Hoefer, Mark A. 2016 Observation of dispersive shock waves, solitons, and their interactions in viscous fluid conduits. *Phys. Rev. Lett.* **116** (17), 174501.

Mo, Y. C., Kishek, R. A., Feldman, D., Haber, I., Beaudoin, B., OShea, P. G. & Thangaraj, J. C. T. 2013 Experimental observations of soliton wave trains in electron beams. *Phys. Rev. Lett.* **110** (8).

Olson, P. & Christensen, U. 1986 Solitary wave propagation in a fluid conduit within a viscous matrix **91**, 6367.

Rothenberg, Joshua E. 1991 Observation of the buildup of modulational instability from wave breaking. *Optics Letters* **16** (1), 18.

Rothenberg, Joshua E. & Grischkowsky, D. 1989 Observation of the formation of an optical intensity shock and wave breaking in the nonlinear propagation of pulses in optical fibers. *Phys. Rev. Lett.* **62** (5), 531.

Scott, David R., Stevenson, David J. & Whitehead, John A. 1986-02 Observations of solitary waves in a viscously deformable pipe. *Nature* **319** (6056), 759–761.

Taylor, R. J., Baker, D. R. & Ikezi, H. 1970 Observation of collisionless electrostatic shocks. *Phys. Rev. Lett.* **24** (5), 206.

Whitehead, John A. & Helfrich, Karl R. 1988-11 Wave transport of deep mantle material **336** (6194), 59.

Whitehead, J. A. & Luther, D. S. 1975 Dynamics of Laboratory Diapir and Plume Models. *Journal of Geophysical Research* **80** (5), 705–717.

Whitham, G. B. 1974 *Linear and nonlinear waves*. Wiley-Interscience [John Wiley & Sons], pure and Applied Mathematics.